Chemical Science

Accepted Manuscript

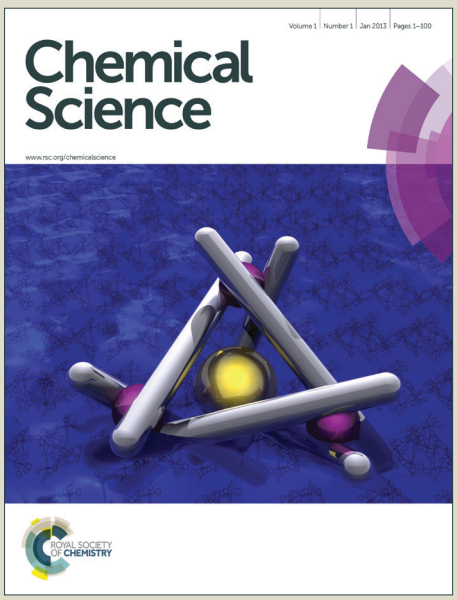

ROYAL SOCIETY OF CHEMISTRY

www.rsc.org/chemicalscience

Cite this: DOI: 10.1039/c0xx00000x

www.rsc.org/xxxxxx

ARTICLE TYPE

Multiscale electrochemistry of hydrogels embedding conductive nanotubes

Jean-Marc Noël,[a] Léopold Mottet,[b] Nicolas Bremond,[b] Philippe Poulin,[c] Catherine Combellas,[a] Jérôme Bibette[b] and Frédéric Kanoufi[a]*

Received (in XXX, XXX) Xth XXXXXXXXX 20XX, Accepted Xth XXXXXXXXX 20XX
DOI: 10.1039/b000000x

The local functionalities of biocompatible objects can be characterized under conditions similar to their operating ones by scanning electrochemical microscopy (SECM). In the case of alginate beads entrapping carbon nanotubes (CNTs), SECM allows evidencing the local conductivity, the organization, and the communication between CNTs. It shows that the CNTs network is active enough to allow long range charge evacuation, enabling the use of alginate/CNT beads as soft 3D electrodes. Direct connection or local interrogation by microelectrodes allows visualizing their communication as a network and eventually studying them individually at the nanoscale.

Introduction

Hydrogels are soft materials mainly composed of water embedding a polymeric matrix. Their wide range of applications, from food industry, drug delivery[1] to tissue engineering,[2] and their rich physicochemical features make them appealing from both fundamental and applied sides. Most of hydrogels are biocompatible by nature are thus well suited for biotechnology uses. As for other polymer based materials, mixing two kinds of macromolecules charges offers extra properties to the final composite such as stretchability [3] or electrical conductivity. [4]

In a different way, conductive hybrid hydrogels can be obtained by dispersing mineral charges, such as carbon nanotubes.[5] Moreover, incorporating conductive particles opens the way to advanced conducting materials for energy storage,[6,7] biosensors[8] or synthetic tissues.[9] In the design of such smart functional materials, it is then important to assess the availability of their functionalities, particularly *in situ* while they are operated. Owing to the various shape, softness and composition (>90% of water) of hydrogels, SEM or AFM are much less well adapted for imaging their structure without physical disturbance than Scanning Electrochemical Microscopy, SECM, since for SEM, water has to be removed whilst for AFM, there is a contact between the tip and the surface. Conversely, SECM is an *in situ* local (electro) chemical probe technique that is well adapted to smart soft objects imaging. SECM successfully allowed the characterization of soft spherical objects such as polymeric microbeads[10] or vesicles.[11-13] Regarding permeable materials, SECM is able i) to reveal ion transport through a nanoporous membrane,[14] with capability of preferential transport path imaging[15] or, ii) to quantify local conductive sites at an interface.[16,17] Local electrochemical probe microscopies such as SECM or scanning electrochemical cell microscopy, SECCM, are ideal to characterize *in situ* the conductive properties of materials such as CNTs based materials going from single CNTs[17,18] to CNTs networks.[19,21] Only few approaches are reported to study the electrochemical activity of CNTs, or other graphene-like materials, mixed with polymers,[22,23] even though CNTs offer promising strategies for the development of novel methodologies for the formulation of energy storage materials.

Herein, we have focused on auto-organized spherical soft objects engineered from carbon nanotubes (CNTs) and an alginate biopolymer owing to a millifluidic droping method. We have quantified and imaged *in situ* the active sites of such as-formed functional permeable objects by SECM. The ultramicroelectrode (UME) tip of the SECM will be especially used to i) probe actuable hydrogel beads under operation conditions, ii) quantify the increase in conductivity upon CNTs incorporation, iii) characterize the organization of the conductive network and, iv) show how it can be used to directly address or connect the conductive network.

Results and discussion.

SECM approach toward a conductive permeable hydrogel.

As described in the Electronic Supplementary Information (Fig. S1†), multi-walled carbon nanotubes are sonicated with sodium dodecylsulfate then mixed with alginate. This solution is dropped into a calcium bath to create alginate/CNT beads. Such 3 mm diameter alginate beads modified with different percentages of CNTs (0 to 1 weight %) were characterized by SECM in the feedback mode in a solution containing a redox mediator, namely ferrocene methanol (FcMeOH) (Figure 1A). In this mode, an UME tip oxidizes the redox mediator while it is approached to the alginate bead. Far from the object, it produces a steady-state current (i_{inf}) that is limited by the redox mediator diffusion. In the

vicinity of the object and if the latter has conductive properties, the redox mediator is regenerated to its pristine state, yielding a feedback current at the UME tip. The evolution of the normalized tip current, $I = i/i_{inf}$, with the tip-object separation distance, d (also in a normalized form $L = d/a$ with a the UME tip radius), gives the so-called approach curve. As alginate beads are biocompatible and mostly used in aqueous media, the analysis of their conductive properties is performed in water. Indeed, SECM approach curves on the beads were carried out in a KCl medium containing FcMeOH as the redox probe.

The approach curve recorded at an alginate bead free of CNT (Figure 1B, thick light green curve, O) is different from the one corresponding to the classical insulating behavior.[15] This difference is attributed to the partition of FcMeOH between the aqueous phase and the hydrogel and its transport in both phases. Indeed, an approach curve recorded at the hydrogel bead from a water-immiscible solvent (benzonitrile, BZN), with a hydrophobic redox probe (decamethylferrocene, DcFc, Fig. S2†) presents the insulating behavior (negative feedback), which means that the redox mediator does not permeate the alginate bead and no charge transfer occurs at the alginate/BZN interface. Thus, as proposed in earlier works,[24-28] the partition process can be quantitatively described through multiphysics modeling of the approach curve. In the absence of CNT, the experimental curve fits well a theoretical insulating porous behavior (Figure 1B, dark green line).

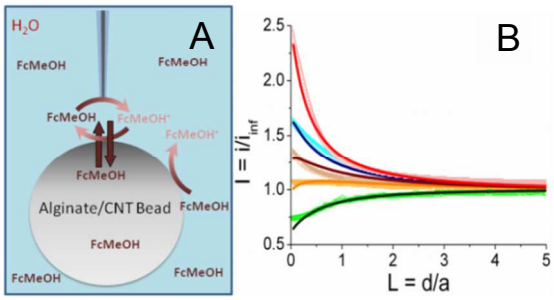

Fig. 1. A) Principle of SECM approach curves on a 2 mm diameter alginate/CNT bead in a 0.1 M KCl + 1 mM $CaCl_2$ aqueous solution containing 1 mM FcMeOH. B) Approach curves recorded with a 12.5 µm Pt UME tip toward alginate beads containing CNTs: 0 (O), 0.13 (O), 0.3 (□), 0.55 (□), and 1 (□) weight %. Dark lines are the simulated curves for irreversible electron transfer kinetics. k_{el} = 0, 1.82, 3.65, 6.08, 12.2 x10^{-3} cm^{-1} for, respectively, 0, 0.13, 0.3, 0.55, 1 wt%, using D = 7.8×10^{-6} $cm.s^{-1}$ for the diffusion coefficient of FcMeOH in water.

When CNTs are added inside the hydrogel beads (from 0.13 to 1 wt%), approach curves show higher feedback currents than in the former insulating case, as the redox mediator is regenerated at the alginate/CNT bead surface (Figure 1B). A feedback current is detected at the tip for a CNTs concentration as low as 0.13 wt% and this feedback increases with the CNTs concentration.

A quantitative estimate of the feedback and therefore of the apparent interfacial charge transfer for each bead composition is provided by modelling the data through permeation of the redox species in the alginate bead phase and interfacial electron transfer process (regeneration of FcMeOH) at the water/bead interface. The permeation allows taking into account for the higher reservoir of redox probe provided by the bead. The apparent interfacial ET averages reasonably the contribution from regeneration within the volume of the bead. As a first approach, we believe that this model is sufficient. Indeed, owing to the size of the UME (25µm diameter) and the diffusion coefficient of the redox probe within the hydrogel, which is about 3 times lower than in aqueous media, the redox probe will be regenerated within than 10µm deep inside the hydrogel and could considered as a weak contribution of the homogeneous phase. This simple theoretical framework yields a reasonable fit of the experimental approach curves as shown in Figure 1B. Noteworthy some deviation between the experimental and the fitted approach curve can be observed, in Figure 1B, at bead containing 0.3% CNT. This could suggest that the regeneration of the redox probe outside the area of the UME is limited. This imbalance could be created in the case of an inhomogeneous repartition or accessibility of the CNTs at the surface (as attested later in the SECM image provided in Figure 2A) or inside the bead. This could be paralleled to systems for which the probed conductor is not much larger than the tip.[29] However, this interpretation is at this point speculative and probably true only for a low percentage of CNT since at 1% CNT the accessibility of CNT is homogeneous, (as also confirmed by SECM image discussed later in Figure 2B).

Even if a more refined model considering homogeneous charge transfer within the bead phase and requiring at least 2 other adjustable parameters would be more complete, the fit provided by the simplest model is reasonable, as was also suggested in other related systems combining layers of polymer embedding CNTs.Moreover, in the literature, the irreversible charge transfer model appeared to be a well adapted approach to study nanoparticles or carbon nanotubes trapped at various interfaces[19,30-35] More notably, the apparent charge transfer rate constant determined from the approach curves fitting increases linearly with the percentage of CNTs trapped inside the hydrogel. Moreover, the increase of FcMeOH concentration does not increase the charge transfer rate (not shown). These observations on the charge transfer process at the bead surface upon CNTs incorporation suggest that conductive sites, likely CNTs arranged in a nanoelectrodes network, are now exposed and available at the bead surface to the solution phase. As the bead is not connected to any electrical source, the observation of a steady-state charge transfer at the bead surface also indicates that upon redox mediator regeneration (reduction of FcMeOH by the CNTs), charges (electrons and ions) are readily propagated within the bead to be evacuated toward the solution or deeper in the bead (by oxidation of FcMeOH, see Figure 1A) at distances larger than the UME tip size.

2D SECM conductivity images.

SECM also allows the imaging of the distribution of the reactive sites responsible for the surface conductivity of the outer membrane of the alginate/CNT beads. Using the same 12.5 µm radius UME tip, the image at the apex of a bead containing 0.55 wt% CNT (Figure S3A†) recorded in a FcMeOH aqueous medium presents a homogeneous conductivity (in line with the reproducibility of the approach curves performed on different locations). With a nanoelectrode (nanotip, 400 – 500 nm radius),[36,37] a higher resolution is expected for the

electrochemical image of the bead. Few individual small conductive spots with 5-10 µm FWHM diameter (~ 6 µm, in inset) are revealed at beads containing 0.3 wt% of CNTs, as shown in Figure 2A, whereas the density of these active regions significantly increases when the CNT wt% entrapped inside the gel increases to 0.55 (Figure SI3B) and 1 wt% (Figure 2B).

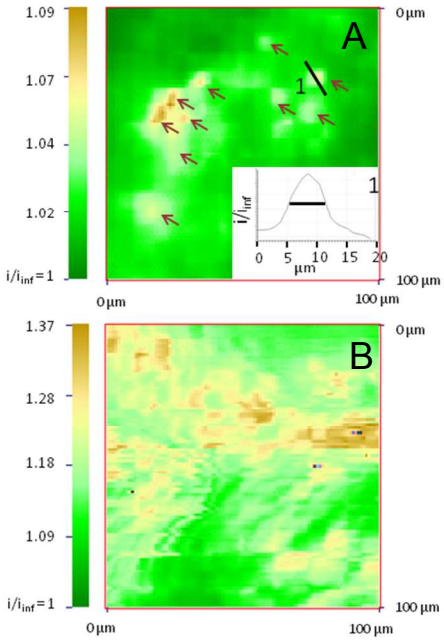

Fig. 2. SECM images recorded on alginate/CNT beads in a 0.1 M KCl + 1 mM $CaCl_2$ aqueous solution containing 1 mM FcMeOH + A) 0.3 and B) 1 wt% CNTs. 400 nm – 500 nm radius Pt nanotip at a 10 µm.s^{-1} velocity. The nanotip is kept at less than 1 µm from the surface. The current scale is normalized by the steady state current recorded in the bulk solution. In Figure 2A, the arrows point the 10 most conductive spots and the inset shows the current profile along the black line on one spot.

At low concentrations of CNTs, the SECM images show that only few agglomerates are exposed directly to the external solution and work as a network of individual microelectrodes. Assuming each spot acts as an individual microelectrode, their size can be estimated from the maximum feedback they sustain (measured in Figure 2A),[38] and can be compared to the theoretical values obtained from finite elements. Typically, the ten intense spots resolved in Figure 2A with i/i_{inf} in the 1.03-1.09 range (see arrows) correspond to feedback responses of individual microelectrodes separated by 1 µm from a 1 µm diameter nanotip with an apparent diameter in the 1-1.5 µm range. This is in reasonable agreement with Figure 2A since, due to convolution with the tip size, the SECM image of these individual microelectrodes would ideally be 2-3 µm diameter active spots.

Noteworthy, the density of these active sites (40-50 µm^2 over a 10^4 µm^2 image) is within the 0.3 % density of the CNTs incorporated in the bead. The spacing between each of these active spots is higher than the nanotip dimension used for their imaging in Figure 2A. This strongly suggests that if these spots are detected electrochemically with both 1 and 12.5 µm radius tips, they are connected to each other for charge evacuation.

The contrast and density of the apparent active sites revealed in the SECM images also reflect the overlapping of the diffusion layers generated by the network of microelectrodes formed by the CNTs assemblies. It allows imaging the individual location of the spots and also their range of cross-talk. For a low concentration of CNTs, the overlapping of the diffusion layers of the microelectrodes network is evidenced and limited to the upper part of Figure 2A. The increase of the CNTs concentration results in an apparent increase of the number of conductive spots and significant overlapping of the diffusion cross-talk, as shown in Figure S3B† and Figure 2B for 0.55 and 1 wt% CNT beads respectively. The feedback ($1.09 < i/i_{inf} < 1.37$) recorded over the whole imaged surfaces is significant and compares to the maximum expected current for a positive feedback for d = 1 or 0.5 µm (i/i_{inf} = 1.25 or 1.57, respectively). The full regeneration of the redox probe at the bead is then detected by the SECM nanotip over regions expanding over several tens of µm^2, showing the large interpenetration of the active spots fields of action. It then suggests that the bead with 1 wt% CNT is comparable to an arrays of nanoelectrodes, which behave as a "macroelectrode", owing to the overlapping of the individual diffusion layers.[38,39] The features, which are imaged in Figure 2B, could then reveal the topography of the macroelectrode and therefore the topography of the bead surface, where the regions of higher current are overhanging by as much as 1 µm the lower current regions. The difference between Figures 2A and B further suggests the CNTs assembly is homogeneously distributed at high CNT concentrations and more segregated at lower concentrations. Finally, both SECM images and approach curves show that the CNTs entrapped in an alginate bead behave as macro- or micro- electrode arrays. Definitely, such an observation requires that charge evacuation occurs efficiently within the bead, certainly through a percolated CNTs network entrapped within the hydrogel. If micro- or nano- electrochemical probes allow evidencing and imaging the structure of the CNTs percolation in the hydrogel beads, the macroscopic range of the charge transfer (or percolation) within the bead can be explored by direct electrical connection of the bead.

Connection to the conductive network.

Penetrating the UME tip inside the bead allows inspecting the extent of this conductive network within the alginate bead. The approach curve from the solution to the bead interior is depicted in Figure SI4† where the solution/bead interface is indicated as the red vertical line; the deeper the penetration into the bead, the higher the feedback current. After ~ 50 µm penetration inside the bead, the tip current increases by several orders of magnitude (from 2 nA in the solution to several µA), suggesting that the UME tip has electrically connected the CNTs percolated network. It is then no more possible to interrogate the micro environment of the tip but only the entire range of the percolated network functioning as a macroelectrode.

One interest of using a UME for this connection is the large increase of current from the transition between a microelectrode and macroelectrode behaviour. Another is also from the ability to connect reversibly the percolated network without too much physical perturbation of the object (experimental details in SI).

It is interesting to note here that no significant increase in the

current has been detected during the connection to 0.13, 0.3 and 0.5 wt% CNT beads, traducing an efficient percolation detected between 0.5 and 1 wt%.

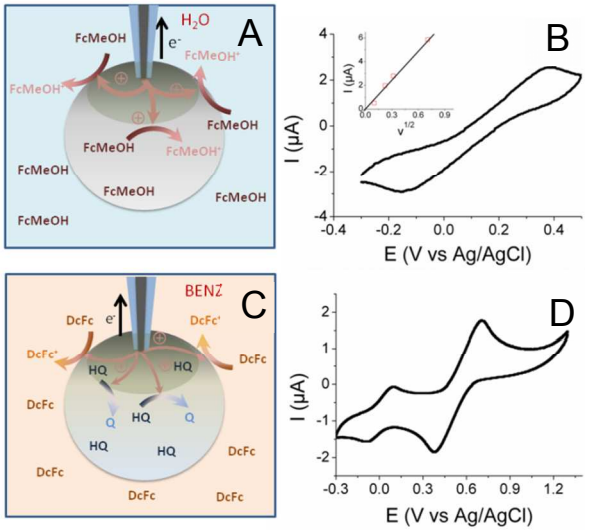

Fig. 3. A, C) Principle of direct connection of an alginate bead with a 12.5 µm radius UME tip. B, D) Cyclic voltammograms recorded at a 3 mm diameter alginate bead containing 1 wt% CNT: B) in a 0.1 M KCl + 1 mM FcMeOH aqueous solution at a scan rate v = 100 mV.s^{-1} (inset: peak current, Ip, as a function of v$^{1/2}$); C) equilibrated with an aqueous solution of 1 mM Hydroquinone (HQ) and immersed into a 1 mM DcFc + 0.1 M NBu_4BF_4 BZN solution.

The principle of the connection between the UME tip and the CNTs network in a 1 wt% CNT bead is illustrated in Figure 3A together with the resulting cyclic voltammogram (CV) of FcMeOH oxidation (Figure 3B). It would be interesting to compare the charge transfer capacities of the beads obtained either probe approach curves, Figure 1, obtained at different concentrations of CNTs with CVs recorded at different CNT contents; unfortunately it was not possible to connect properly the conducting network with the UME for a concentration below 1%, probably because of the limited accessibility of the CNT network at low percentage of CNT and higher resistance of the bead. This particularly highlights the unique potentiality of SECM to address the electrochemical activity of such soft objects with low conductivity.

The CV shows the classical response expected for a macroelectrode, except that the peak to peak separation potential, ΔE_p = 536 mV at v = 100 mVs^{-1}, is largely higher than the theoretical value obtained at a classical metallic electrode for a diffusion process (ΔE_p = 60 mV). This behavior traduces a large charge transfer resistance probably due to a limited accessibility of the deeper regions of the CNTs network. However, this experiment clearly shows the possibility to connect the CNTs network trapped inside the hydrogel. The peak current (Ip) also varies linearly with v$^{1/2}$ (inset in Figure 3B). Even if the electrochemical response shows considerable ohmic contribution, the Ip-v$^{1/2}$ response may suggest diffusion-controlled limitation. From this experiment and using the FcMeOH diffusion coefficient in alginate as $D_{FcMeOH\ /Alg}$ = 2.9x10^{-6} cm².s^{-1}, both the equivalent resistance and surface area of the connected 1 wt% CNTs network can be estimated from simulation of the CVs (see SI). The UME-bead electrical contact is equivalent to a 3.3 mm² electrode of 80 kΩ resistance. This means that by contacting the bead, the active area of the UME tip used as a connector is multiplied by 6.7x10^3. Such a significant increase shows a volumetric percolation of the CNTs network through the bead. Of course, since the cyclic voltammetry was recorded in an aqueous medium and due to the high permeability of the bead, the CV may result from the response of a volume fraction of the bead.

A further picture of the electrochemical characteristic for the alginate/CNT bead is obtained by separating the outer surface and the bulk bead contributions. For this purpose, a bead was equilibrated in a hydroquinone (HQ) solution and then immersed into a BZN electrolyte containing DcFc as a redox probe (Figure 3C). The CV obtained by the same electrical connection to an UME tip (Figure 3D) shows two reversible waves corresponding to the response of both the redox probe (DcFc in the BZN phase) and HQ (inside the hydrogel). This clearly shows that it is possible to connect the outer surface of the bead from its interior (the electrode was inserted <100 µm inside the bead), showing a long distance percolation range of the CNTs network. A more quantitative estimate of the equivalent electroactive surface area is obtained for the outer surface (from the DcFc CV) and the volumetric network (from the HQ CV) of the bead from the respective peak current analysis. It ensures that 0.3 mm² of the external surface of the bead is active (using $D_{DcFc/BZN}$ = 4.6×10^{-6} cm².s^{-1} for DcFc diffusion in BZN), which corresponds to 1% of the surface of the bead. Due to the large overlapping of the active nanodomains formed by the CNTs network evidenced by SECM, this value suggests that the electrical connection is effective for electrochemical measurements over the 1% area in the vicinity of the electrical connection. Typically, the UME tip addresses here an electrically connected region equivalent to a 0.3 mm radius disk electrode. Conversely, the part of the CNTs network connected within the interior of the bead has an active area of 0.8 mm² (considering $D_{HQ/Alg}$ = $D_{FcMeOH/Alg}$ = 2.9x10^{-6} cm².s^{-1}). The electrically connected alginate/CNT bead then behaves as a macroscopic porous electrode. From the area connected at the outer surface, it is anticipated that the electrical connection inside the bead expands only over a hemisphere of similar radius (0.3 mm). Such a percolated porous electrode then behaves as a 0.3 mm hemisphere electrode, leading to a 2-fold increase of the inside electroactive area, in reasonable agreement with the 2.6-fold increase observed.

Conclusions

These preliminary investigations show all the interest of the SECM to characterize the availability of physical or chemical functionalities of smart, soft, biocompatible objects, under conditions similar to their operating ones, without physical perturbation, which is very important to keep the structure of the composite. Thus, approach curves performed with an UME tip at the surface of a hydrogel bead entrapping CNTs allows easily characterizing their local conductivity. High resolution SECM imaging clearly evidences the local availability, the organization, and the communication of the functional objects entrapped within

the composite (here CNTs modified hydrogel beads). At low contents, the CNTs assemble in individual segregated bundles of approx. 5 µm diameter. The bead is then not conductive enough to be addressed electrochemically by CV which highlights the unique proficiency of SECM for the electrochemical characterization of such poorly conductive soft objects. At higher concentrations, the CNTs distribution is more homogeneous and the bead is a dense overlapping network of nanoelectrodes, which behaves as a rough macroelectrode. In all cases, the CNTs network is active enough to allow long range charge evacuation, enabling the use of alginate/CNT beads as soft 3D electrodes. This is confirmed from the direct connection of the CNTs network with the UME tip. It is then possible to address with a 12.5 µm radius UME inserted inside the bead the whole electrical volume or surface in a liquid/liquid environment within a range of 300 µm from the tip-bead contact. The use of this 3D biocompatible hydrogel can be extended to the trapping and further electrochemical addressing of many other kinds of objects, such as nanoparticles, electroactive molecules or biological entities. The direct connection or local interrogation by microelectrodes allows visualizing their communication as a network and eventually studying them individually at the nanoscale. The potentiality of such hydrogels in a liquid/liquid environment is also demonstrated, which is appealing in the development of soft materials for energy storage/release.

Acknowledgments.

This work was supported by Université Paris-Diderot, ESPCI and CNRS.

Author contribution.

The first two authors contributed equally to this work.

Notes and references

[a] *Sorbonne Paris Cité, Paris Diderot University, Interfaces, Traitements, Organisation et Dynamique des Systèmes (ITODYS), CNRS-UMR 7086, 15 rue J. A. Baif, 75013 Paris – France. fax : 33157277263. tel 33157277217 frederic.kanoufi@univ-paris-diderot.fr.*

[b] *Laboratoire Colloïdes et Matériaux Divisés, from the Institute of Chemistry, Biology and Innovation (CBI) - ESPCI ParisTech / CNRS-UMR8231 /PSL* Research University, 10 rue Vauquelin 75231 Paris Cedex - France*

[c] *Centre de Recherche Paul Pascal – CNRS, University of Bordeaux, 115 Avenue Schweitzer, 33600 Pessac - France.*

† Electronic Supplementary Information (ESI) available: alginate/carbon nanotubes beads fabrication and optical image, SECM approach curves in benzonitrile, 2D conductivity images, SECM when the tip penetrates inside the bead and Digisim® simulation of cyclic voltammograms obtained at UME inside a 1% CNT bead.

1 T. R Hoare, D. S. Kohane, *Polymer* **2008**, *49*, 1993.
2 K. Y. Lee, D. J. Mooney, *Chem. Rev.*, 2001, **101**, 1869.
3 J.-Y. Sun, X. Zhao, W. R. K. Illeperuma, O. Chaudhuri, K. H. Oh, D. J. Mooney, Z. Suo, *Nature*, 2012, **489**, 133.
4 A. Guiseppi-Elie, *Biomaterials*, 2010, **31**, 2701.
5 Z. Yang, Z. Cao, H. Sun, Y. Li, *Adv. Mater.*, 2008, **20**, 2201.
6 H. Wu, G. Yu, L. Pan, N. Liu, M.T. McDowell, Z. Bao, Cui Y. *Nature Commun.*, 2013, **4**, 1943.
7 B. Liu, P. Soares, C. Checkles, Y. Zhao, G. Yu, *Nano Lett.*, 2013, **13**, 3414.
8 D. Zhai, B. Liu, Y. Shi, L. Pan, Y. Wang, W. Li, R. Zhang, G. Yu, *ACS nano*, 2013, **7**, 3540.
9 R. A. MacDonald, C. M. Voge, M. Kariolis, J. P. Stegemann, *Acta Biomater.*, 2008, **4**, 1583.
10 C. N. Kirchner, M. Träuble, G. Wittstock, *Anal. Chem.*, 2010, **82**, 2626.
11 W. Zhan, A. J. Bard, *Anal. Chem.*, 2006, **78**, 726.
12 D. Correia-Ledo, A. A. Arnold, J. Mauzeroll, *J. Am. Chem. Soc.*, 2010, **132**, 15120.
13 R. Tomasi, J.-M. Noël, A. Zenati, S. Ristori, F. Rossi, V. Cabuil, F. Kanoufi, A. Abou-Hassan, *Chem. Sci.*, 2014, **5,** 1854**.**
14 M. Shen, R. Ishimatsu, J. Kim, S. Amemiya, *J. Am. Chem. Soc.*, 2012, **134**, 9856.
15 A. J. Bard, M. V. Mirkin, Eds.; Scanning Electrochemical Microscopy; Taylor & Francis: New York, 2012.
16 J. Azevedo, C. Bourdillon, V. Derycke, S. Campidelli, C. Lefrou, R. Cornut, *Anal. Chem.*, 2013, **85**, 1812.
17 J. Kim, H. Xiong, M. Hofmann, J. Kong, S. Amemiya, *Anal. Chem.*, 2010, **82**, 1605.
18 A. G. Güell, K. E. Meadows, P. V. Dudin, N. Ebejer, J. V. Macpherson, P. R. Unwin, *Nano Lett.*, 2014, **14**, 220.
19 N. R. Wilson, M. Guille, I. Dumitrescu, V. R. Fernandez, N. C. Rudd, C. G. Williams, P. R. Unwin, J. V. Macpherson, *Anal. Chem.*, 2006, **78**, 7006.
20 T. S. Miller, N. Ebejer, A. G. Güell, J. V. Macpherson, P. R. Unwin, *Chem. Commun*., 2012, **48**, 7435.
21 A. G. Güell, N. Ebejer, M. E. Snowden, K. McKelvey, J. V. Macpherson, P. R. Unwin, *Proc. Natl. Acad. Sci. USA*., 2012, **109**, 11487.
22 V. A. Pedrosa, T. Gnanaprakasa, S. Balasubramanian, E. V. Olsenc, V. A. Davis, A. L. Simonian, *Electrochem. Commun*., 2009, **11**, 1401.
23 M. E. Snowden, M. A. Edwards, N. C. Rudd, J. V. Macpherson, P. R. Unwin, *Phys. Chem. Chem. Phys.*, 2013, **15**, 5030.
24 A. L. Barker, P. R. Unwin, *J. Phys. Chem.*, 2001, **105**, 12019.
25 P. Bertoncello, I. Ciani, D. Marenduzzo, P. R. Unwin, *J. Phys. Chem. C*, 2007, **111**, 294.
26 C. Cannes, F. Kanoufi, A. J. Bard, *Langmuir*, 2002, **18**, 8134.
27 J. Guo, S. Amemiya, *Anal. Chem.*, 2005, **77**, 2147.
28 J. Kim, A. Izadyar, N. Nioradze, S. Amemiya, *J. Am. Chem. Soc.*, 2013, **135**, 2321.
29 A. I. Oleinick, D. Battistel, S. Daniele, I. Svir, C. Amatore, Anal. Chem., 2011, 83, 4887.
30 J. Zhang, R. M. Lahtinen, K. Kontturi, P. R. Unwin, D. J. Schiffrin, *Chem. Commun.*, 2001, 1818.
31 B. M. Quinn, I. Prieto, S. K. Haram, A. J. Bard, J. Phys. Chem. B, 2001, **105**, 7474.
32 P. Liljeroth, D. Vanmaekelbergh, V. Ruiz, H. Jiang, E. Kauppinen, B. M. Quinn, *J. Am. Chem. Soc.*, 2004, **126**, 7126.
33 P. G. Nicholson, V. Ruiz, J. V. Macpherson, P. R. Unwin, Phys. Chem. *Chem. Phys.*, 2006, **8**, 5096.
34 F. Li, I. Ciani, P. Bertoncello, P. R. Unwin, J. Zhao, C. R. Bradbury, D. J. Fermin, *J. Phys. Chem. C*, 2008, **112**, 9686.
35 J.-M. Noël, D. Zigah, J. Simonet, P. Hapiot, Langmuir, 2010, 26, 7638.
36 B. Ballesteros Katemann, W. Schuhmann, *Electroanalysis,* 2002, **14**, 22.

37 J. Velmurugan, P. Sun, M. V. Mirkin, *J. Phys. Chem. C*, 2009, **113**, 459.
38 C. Amatore, J.-M. Savéant, D. Tessier, *J. Electroanal. Chem. Interfacial Electrochem.*, 1983, **147**, 39.
39 N. Godino, X. Borrisé, F.X. Muñoz, F.J. del Campo, R.G. Compton, *J. Phys. Chem. C*, 2009, **113**, 11119.